Journal of Flow Chemistry
https://doi.org/10.1007/s41981-021-00172-3

FULL PAPER

Continuous citrate-capped gold nanoparticle synthesis in a two-phase flow reactor

Spyridon Damilos[1] · Ioannis Alissandratos[2] · Luca Panariello[1] · Anand N. P. Radhakrishnan[1] · Enhong Cao[1] · Gaowei Wu[1] · Maximilian O. Besenhard[1] · Amol A. Kulkarni[3,4] · Charalampos Makatsoris[2] · Asterios Gavriilidis[1]

Received: 22 January 2021 / Accepted: 27 April 2021

Abstract

A continuous manufacturing platform was developed for the synthesis of aqueous colloidal 10–20 nm gold nanoparticles (Au NPs) in a flow reactor using chloroauric acid, sodium citrate and citric acid at 95 °C and 2.3 bar(a) pressure. The use of a two-phase flow system – using heptane as the continuous phase – prevented fouling on the reactor walls, while improving the residence time distribution. Continuous syntheses for up to 2 h demonstrated its potential application for continuous manufacturing, while live quality control was established using online UV-Vis photospectrometry that monitored the particle size and process yield. The synthesis was stable and reproducible over time for gold precursor concentration above 0.23 mM (after mixing), resulting in average particle size between 12 and 15 nm. A hydrophobic membrane separator provided successful separation of the aqueous and organic phases and collection of colloidal Au NPs in flow. Process yield increased at higher inlet flow rates (from 70 % to almost 100 %), due to lower residence time of the colloidal solution in the separator resulting in less fouling in the PTFE membrane. This study addresses the challenges for the translation of the synthesis from batch to flow and provides tools for the development of a continuous manufacturing platform for gold nanoparticles.

Keywords Nanomaterials · Continuous manufacturing · Online analysis · Segmented flow · Phase separation

Introduction

The unique properties of gold nanoparticles (Au NPs) have instigated research in their biomedical applications [1], drug delivery [2] and antimicrobial applications [3]. This has led to the need for robust and sustainable manufacturing platforms for the delivery of high quality, uniform shape and monodisperse Au NPs. These applications have also been driving the demand for translation from lab-scale synthesis to scalable production and for further downstream processing for appropriate functionalisation [4]. In the past years, there have been several attempts for the translation of batch Au NPs syntheses towards continuous flow processing. Single-phase micro- and milli-reactors have been investigated due to the rapid heat and mass transfer and minimising particle size distribution [5]. Wagner and Köhler [6] used a continuous flow microreactor for the reduction of $HAuCl_4$ with ascorbic acid for the synthesis of 5–50 nm Au NPs capped with polyvinylpyrrolidone (PVP). However, they identified that during the process there was particle deposition (fouling) on the reactor walls, affecting the particle quality. Huang et al. [7] examined the

Highlights
- A continuous segmented flow reactor for gold nanoparticle synthesis has been developed.
- Continuous phase separation and online analysis for nanoparticle size and yield determination have been implemented.
- The platform was used to produce nanoparticles with targeted size in the 10–20 nm range.

✉ Asterios Gavriilidis
a.gavriilidis@ucl.ac.uk

[1] Department of Chemical Engineering, University College London, Torrington Place, London WC1E 7JE, UK

[2] Department of Engineering, Faculty of Natural & Mathematical Sciences, King's College London, London WC2R 2LS, UK

[3] Chemical Engineering & Process Development Division, CSIR-National Chemical Laboratory, Pune 411008, India

[4] Academy of Scientific and Innovative Research (AcSIR), CSIR-National Chemical Laboratory (NCL) Campus, Pune 411008, India

Published online: 06 August 2021

observed particle deposition in fluorinated capillary reactors, showing that fouling consisted of unreacted gold-reducing agent complexes and Au^0 – namely "dark fouling" – and synthesised Au NPs – namely "pink fouling".

Milli-fluidic devises can be used for the scale-up of nanoparticle synthesis, increasing the channel dimension by one order of magnitude, providing similar control over fluid flow and residence time distribution and presenting similar advantages as microfluidic systems [8]. Lohse et al. [9] implemented a milli-fluidic reactor comprising of a polyethylene Y-mixer connected to a TYGON polyvinyl tubing (inner diameter: 2.7 mm) and an online UV-Vis spectrometer at the outlet of the reactor for the monitoring of the synthesised gold nanoparticles. The reactor could be used for the synthesis of aqueous spherical citrate-, ω-functionalized thiol- and CTAB-stabilised gold nanoparticles, 2–40 nm in size, via $NaBH_4$ reduction of $HAuCl_4$, as well as for the synthesis of gold nanorods, 15–50 nm in length and aspect ratio between 1.5 and 4, and gold nanocubes. Varying the length of the tubing (and subsequently the volume of the reactor), the residence time could be varied between 3 and 30 min without changing the flow velocity and avoiding fouling. In recent years, there has also been an increasing interest towards the application of methods for rapid quality control [10, 11] (including for example online UV-Vis absorption spectroscopy [12, 13]) to ensure the manufacturing of high quality particles and the translation of nanoparticle synthesis from lab-scale towards commercial scale. Baber et al. [14] examined the synthesis of citrate-capped Au NPs via the *Turkevich* method using a coaxial flow reactor (CFR) comprising of an outer glass tube of (inner diameter: 2 mm) and an inner glass tube (inner diameter: 0.8 mm) to minimise the fouling observed during Au NPs synthesis. A coiled flow inverter comprising of a PTFE tube (inner diameter: 1 mm) was used in series with the CFR to improve the residence time distribution. Increasing the flow rate from 0.25 ml/min to 3 ml/min particle size increased from 17.9 ± 2.1 nm to 23.9 ± 4.7 nm, while polydispersity increased from 11 % up to 20 %.

The use of multiphase flow by introduction of an immiscible phase (i.e., organic solvent) has been studied for the elimination of fouling on the reactor walls, due to the formation of a surrounding film around the droplets. Additionally, each formed droplet can be considered as an individual fully mixed reactor that moves along the tube length, making it analogous to plug-flow reactors, hence leading to narrow residence time distribution [15], as well as enhancing the mixing efficiency of the reactants due to the internal vortex circulation [16]. Duraiswamy and Khan [17] used a poly(dimethyl siloxane) (PDMS) microfluidic device (channel depth x width: 155 μm x 300 μm), for the anisotropic synthesis of gold nanostructures. A T-junction allowed the simultaneous addition of the three streams (gold seeds, premixed gold precursor with capping agent (CTAB) and the ascorbic acid acting as reducing agent) forming homogeneous droplets, using silicon oil as the segmenting fluid. Varying reactant concentrations and flow rates resulted in a tunable synthesis of gold nanorods and nanospheres, as well as cubes, tetrapods, and four-edged stars. Sebastian Cabeza et al. [18] studied the reduction of $HAuCl_4$ by $NaBH_4$ for the synthesis of Au NPs (aqueous phase) in a silicon microreactor (channel depth x width: 400 μm x 400 μm) segmented by air, toluene or silicone oil. Due to the hydrophilicity of the silicon channels, water was the continuous phase. The smallest particles were synthesised in the air-water system (2.8 ± 0.2 nm), while the silicon oil-water system resulted in a bimodal particle size distribution (7.8 ± 6.5 and 15.5 ± 3.1 nm). The air-water system provided the best internal recirculation in the aqueous slugs, improving the residence time distribution. Kulkarni and Sebastian Cabeza [19] compared the toluene-water two-phase flow in a hydrophobic PTFE capillary reactor (inner diameter: 2.5 mm) and a hydrophilic microreactor (similar to Sebastian Cabeza et al. [18]). Two-phase flow using toluene as the continuous phase (the colloidal Au NPs were formed in the aqueous disperse phase) avoided fouling on the hydrophobic capillary walls, but absorption of the particles at the liquid-liquid interface was observed. Carino et al. [20] developed a segmented flow tubular reactor (SFTR) for the synthesis of citrate-capped spherical Au NPs. Operating at 95 °C with 5 min residence time, yielded monodisperse particles of ~ 15 nm in size. The throughput could potentially increase up to 5 g/day, followed by ultrafiltration and dialysis for sample purification.

The aim of this work is the targeted synthesis of 10–20 nm citrate-capped Au NPs. A two-phase flow system, using heptane as the continuous phase is used to prevent fouling on the reactor walls. A membrane separator is implemented for the separation and collection of the two phases in flow (the aqueous phase comprising the colloidal Au NPs and the organic phase). An online UV-Vis spectrometer allows live monitoring of the quality of the synthesised nanoparticles and hence assessment of the stability and yield of the manufacturing process.

Experimental section

Materials and methods

The reactants used in this work were citric acid (H_3Ct: $C_6H_8O_7 \cdot H_2O$, Sigma-Aldrich), trisodium citrate (Na_3Ct: $Na_3C_6H_5O_7 \cdot 2H_2O$, Fisher Scientific), Gold (III) chloride trihydrate ($HAuCl_4 \cdot 3H_2O$, Sigma-Aldrich) and n-heptane (≥ 99 %, $CH_3(CH_2)_5CH_3$, Sigma-Aldrich) and were of analytical grade. Basic blue 3 ($C_{20}H_{26}ClN_3O$, Sigma-Aldrich) was used for

the evaluation of the liquid-liquid separation using the membrane separator. Ultra-pure water (15 MΩ·cm) was used for all aqueous solutions in all experiments. Polytetrafluoroethylene (PTFE) tubing (1 mm inner diameter, VICI Jour) was used for all tubing, and ferrules and fittings made of polyether ether ketone (PEEK) (Upchurch) were used for all required connections in the experimental set-up. The online UV-Vis absorption measurements were carried out using a USB2000 + UV-Vis spectrometer (Ocean Optics) connected to a DT-MINI-2-GS deuterium/tungsten lamp light source (Ocean Optics) via the appropriate fibre optics. For the UV-Vis absorption spectra, the sample passed through a 390 μl flow-through quartz cell (176.700-QS, 10 mm optical path length, Hellma Ltd), and spectral analysis was performed in the range of 200–800 nm. The cuvette was cleaned with ultra-pure water and ethanol (Sigma Aldrich) after each experimental run, to ensure there was no remaining sample in the cuvette, which could lead to particle deposition on the cuvette walls.

The synthesised nanoparticles were characterised (offline) via UV-Vis absorption spectroscopy, pH measurement, transmission electron microscopy (TEM) imaging (Jeol 2010–200 kV), differential centrifugal sedimentation (DCS) (CPS 24 000 Disc Centrifuge, CPS Instruments) and microwave plasma atomic emission spectrometry (MP-AES) (4210 MP-AES, Agilent). For the UV-Vis absorption spectra, the sample was placed in a 3 ml quartz cell (10.00 mm QS, Hellma Ltd), and spectral analysis was performed in the range of 200–800 nm. The pH measurements were performed with a SevenCompact pH meter S220 (Mettler Toledo) equipped with an InLab Micro glass electrode. TEM samples were prepared by placing a drop of the stable sample solution onto a carbon-coated 200 mesh copper grid (C200 Cu, EM Resist Ltd), which was let to dry in air. Particle counts from the TEM image analysis was performed via the Pebbles software to ensure accurate and unbiased particle sizing [21]. The Au NPs samples were analysed via DCS (~0.1 ml injected per sample). The assumed nanoparticle density for the DCS analysis was 12.3 g/ml, as it was shown to provide comparable results with TEM image analysis for the range of 8–30 nm citrate-capped Au NPs [22]. In order to evaluate the conversion of the Au precursor, two samples of equal volume were obtained from the collected solution; the first sample was precipitated using 1 M NaCl solution and filtered (using a 0.2 μm pore cellulose-acetate filter, Sartorius Stedim Biotech) and then the filtrate along with the second sample were dried in an over at 105 °C. The dried filtrate and second sample were digested in a solution of 1:9 (by volume) aqua regia:water and the conversion was evaluated by the difference in the concentration of gold Au^0 between the filtrate $\left([Au^0]_{filt}\right)$ and the collected solution $\left([Au^0]_{sol}\right)$ $\left(Conversion = \frac{[Au^0]_{sol} - [Au^0]_{filt}}{[Au^0]_{sol}}\right)$. The yield was also evaluated from the ratio of the Au^0 from the Au NPs in the collected solution over the target concentration of $Au(III)$ after mixing ($Yield = \frac{[Au^0]_{sol} - [Au^0]_{filt}}{[HAuCl_4]_{target}}$).

Experimental set-up

Gold nanoparticles were synthesised in a continuous two-phase flow system, where the colloidal gold nanoparticle solution comprised the dispersed phase, while heptane acted as the continuous phase, in order to avoid nanoparticle deposition on the walls of the PTFE capillary. In the citrate reduction (*Turkevich*) method, the gold precursor ($HAuCl_4$) was reduced by a mixture of citric acid (H_3Ct) and trisodium citrate (Na_3Ct), so as the final pH of the sample was ~5.6 to ensure a highly reproducible synthesis, according to the work by Kettemann et al. [23]. The precursor stock solution that was used was 5 mM $HAuCl_4$, while two freshly prepared stock solutions of 50 mM H_3Ct and 50 mM Na_3Ct were mixed at specific ratios for a given $HAuCl_4$ concentration. Firstly, the two reacting solutions ($HAuCl_4$ and the appropriate mixture of H_3Ct:Na_3Ct) were prepared by filling two glass syringes (25 ml, Scientific Glass Engineering) at predefined concentrations for the synthesis of the targeted nanoparticle size (aqueous phase), based on our previous experimental conditions in batch for the synthesis of 10–20 nm citrate-capped Au NPs (Table 1) [24]. A third glass syringe (50 ml, Scientific Glass Engineering) was filled with heptane (organic phase). The flow of the three solutions was regulated by two syringe pumps (PHD Ultra, Harvard Apparatus). The two aqueous solutions were delivered at the same flow rate ($\dot{V}_{HAuCl_4} = \dot{V}_{H_3Ct:Na_3Ct}$) and the inlet flow rate of each reactant ranged between 0.080 and 0.155 ml/min. The ratio between the total aqueous ($\dot{V}_{Aqueous} = \dot{V}_{HAuCl_4} + \dot{V}_{H_3Ct:Na_3Ct}$) to organic flow rate ($\dot{V}_{Organic}$) was 1:1 ($\dot{V}_{Aqueous} = \dot{V}_{Organic}$) and the flow rate of the heptane stream ranged between 0.16 and 0.310 ml/min. The reactants were mixed at room temperatures (20–25 °C) before entering the heated reactor (shown in Fig. 1).

A coiled capillary was used as mixer consisting of a PTFE capillary of 0.21 ml volume (inner diameter: 0.5 mm, outer diameter: 1.59 mm, length: 1.07 m, VICI Jour). A PEEK T-junction with 0.5 mm through-hole (Upchurch) at the outlet of the mixer allowed droplet generation using heptane as the segmenting fluid. The droplets passed through a 2.25 ml coiled capillary reactor (inner diameter: 1 mm, outer diameter: 1.59 mm, length: 2.87 m, VICI Jour) made of PTFE. A glycerol bath on a hot plate with an integrated magnetic stirrer (Stuart UC152D, Cole-Parmer Ltd) was used for the regulation of the synthesis temperature. The temperature homogeneity in the glycerol bath was evaluated by immersing an external thermocouple at various positions and depths during the synthesis; there were no temperature variations of more than 1 °C from the set temperature of 95 °C. Upon exiting the reactor,

Table 1 $HAuCl_4$, H_3Ct and Na_3Ct concentrations (after mixing), reactants and heptane streams flow rates and nominal residence times in the 2.25 ml reactor for the targeted synthesis of 10–20 nm gold nanoparticles at pH value ~ 5.6

Experimental set	Target Au NPs (nm)	Experimental conditions						
		$[HAuCl_4]$ (mM)	$[H_3Ct]$ (mM)	$[Na_3Ct]$ (mM)	$\dot{V}_{HAuCl_4}$ (ml/min)	$\dot{V}_{H_3Ct:Na_3Ct}$ (ml/min)	$\dot{V}_{Heptane}$ (ml/min)	Nominal residence time (min)
A	10	0.5	1.65	5.85	0.155	0.155	0.310	3.6
B	15	0.23	0.21	1.17	0.09	0.09	0.174	6.5
C	20	0.065	0.10	0.29	0.08	0.08	0.158	7.1

Temperature of synthesis 95 °C [24]

the droplets were cooled using an ice bath before entering the membrane separator in which the top stream contained the aqueous phase of the Au NPs and the bottom stream contained the organic phase. A by-pass stream directed the two-phase flow from the reactor outlet to a waste bottle, when desired. A flow-through cell was connected on the aqueous stream for the online monitoring of the UV-Vis spectra of the Au NPs solution. A 2.3 bar(a) pressure was maintained in the reactor using a backpressure regulator (BPR) (max. 4 bar K-type, Swagelok) connected to a nitrogen cylinder (BOC) to avoid boiling and bubble formation inside the capillary reactor. Collection vessels of the organic phase were connected with a vial filled with activated carbon to prevent heptane vapours from escaping in the environment.

Results & discussion

Hydrodynamics and reactants mixing

A representative schematic of the droplet formation is shown in Fig. 2. During gold synthesis, nanoparticle deposition can occur on the reactor walls in the absence of a hydrophobic film separating the aqueous phase from the PTFE material [7]. As PTFE is hydrophobic [13] and the heptane was the carrier phase, water convex segments were formed, while a liquid film was formed between the aqueous droplets and the capillary walls due to the wetting of the hydrophobic PTFE surface by the organic phase. By varying the flow rates of the aqueous and organic phase (Section S1, Supplementary Information), the droplet size and its standard deviation were evaluated,

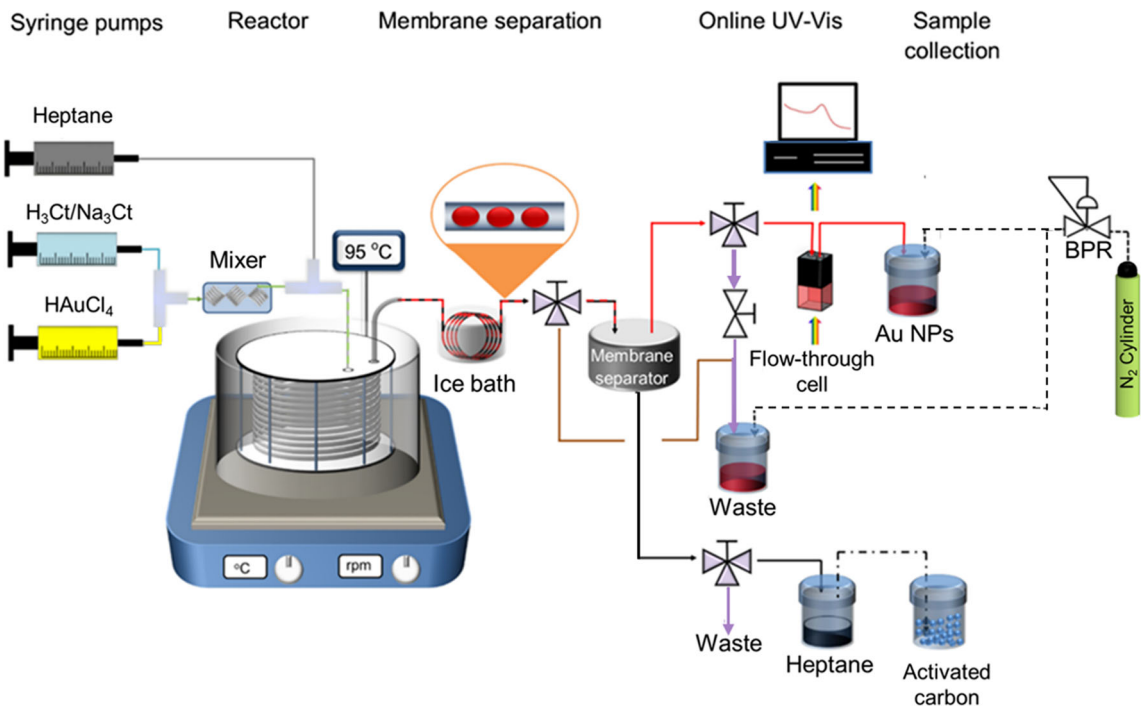

Fig. 1 Setup of the two-phase continuous synthesis system of citrate-capped gold nanoparticles using heptane as a continuous segmenting phase and $HAuCl_4$, H_3Ct:Na_3Ct as reactants

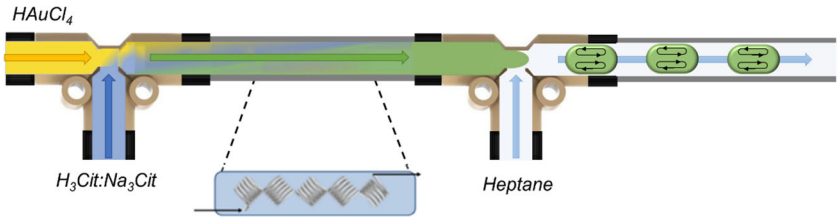

Fig. 2 Schematic representation of the mixing process and the segmented flow in the PTFE capillary. The aqueous streams were mixed at room temperature using a PEEK T-junction followed by a coiled capillary mixer prior to the formation of the aqueous droplets using heptane as continuous phase in the PTFE capillary

since small and uniform droplets are desired to ensure good mixing and narrow residence time distribution to approximate a plug-flow reactor [15] leading to reproducible and monodisperse colloidal gold nanoparticles. The droplet length is affected by the ratio between the aqueous and organic flow rates [25], and by increasing the aqueous flow rate the droplet length increases due to the lower shear stress exerted on the aqueous droplet by the continuous phase [26]. Yue et al. [13] examined the effect of the aqueous-to-organic flow rate ratio in a PTFE capillary microreactor, showing that when increasing the flow rate ratio the length of the aqueous droplet increases in comparison with the length of the organic liquid slug. For $\dot{V}_{Aqueous} = \dot{V}_{Organic}$ ($\dot{V}_{Organic}$ is the flow rate of the organic inlet steam) the lengths of the aqueous droplet and the organic liquid slug were almost equal. In this study, the gold precursor and the $H_3Ct{:}Na_3Ct$ mixture were delivered at the same flow rate ($\dot{V}_{HAuCl_4} = \dot{V}_{H_3Ct:Na_3Ct} = \dot{V}_{Aqueous}/2$) and the aqueous-to-organic flow rate ratio was kept constant and equal to 1:1 ($\dot{V}_{Aqueous} = \dot{V}_{Heptane}$), which ensured uniformly spaced aqueous droplets and heptane slugs and droplet coalescence was avoided.

For the given flow rates (and subsequently the flow velocity of the aqueous-organic system) the capillary number (Ca), the Weber number (We) and the Bond number (Bo) were evaluated to identify the importance of the viscous, inertial and gravitational forces over the interfacial tension forces between the two phases (Section S2, Supplementary Information). The analysis showed that their values were very small ($Ca < 0.0001$, $We < 0.001$, $Bo \approx 0.01$), indicating that the interfacial tension forces were dominant over the viscous, inertial and gravitational forces [27]. In addition, the organic liquid film surrounding the aqueous droplet was negligible compared with the capillary radius (δ = 0.5–1.4 μm for the studied flow rates) and the velocity of the formed droplets could be approximated by the mixture flow velocity [13, 28].

The reactants ($HAuCl_4$ and mixture of $H_3Ct : Na_3Ct$) were mixed at room temperature in a PTFE coiled capillary mixer, prior to segmentation with heptane. For inlet aqueous flow rate from 0.05 to 1 ml/min, the aqueous phase flow can be characterised as laminar, since the Reynolds number varied between 2 and 48. We next define τ_{conv} the time required for the stream to flow from the capillary inlet to outlet, and τ_{diff} a conservative estimate of the time required for the dissolved species to diffuse across the half width of the capillary (Eqs. 1 and 2, respectively) [27, 29]. To evaluate the mixing efficiency of the two aqueous streams, the τ_{conv} and τ_{diff} characteristic times were estimated for a straight capillary of 0.5 mm inner diameter. Centrifugal forces are present in the coiled capillary mixer enhancing the mixing efficiency, but they are not expected to be significant, since the Dean value was ≤ 3 [30, 31]. The aqueous flow rates varied between 0.1 and 1 ml/min. The total aqueous flow rate ($\dot{V}_{Aqueous}$) was equal to the sum of the $HAuCl_4$ ($\dot{V}_{HAuCl_4}$) and water flow rates ($\dot{V}_{Water}$), hence $\dot{V}_{Aqueous} = \dot{V}_{Water} + \dot{V}_{HAuCl_4}$. The molecular diffusivity of gold precursor in water $D_{m,HAuCl_4}$ = $1.4{\cdot}10^{-9}$ m^2/s at 25 °C [32]. The characteristic times are:

$$\tau_{conv} = \frac{L}{u_0} \tag{1}$$

where L is the length of the capillary and u_0 is the average fluid velocity,

$$\tau_{diff} = \frac{\left(\frac{1}{2}d_t\right)^2}{2D_m} \tag{2}$$

where d_t is the inner diameter of the capillary and D_m is the molecular diffusivity of the dilute species. When increasing the average fluid velocity (i.e., aqueous inlet flow rate), τ_{diff} of the gold precursor ($\tau_{diff,\ HAuCl_4}$) remained constant and equal to 22 s, while τ_{conv} decreased from ~ 250 s (for 0.05 ml/min) to 13 s for (for 1 ml/min). When $\tau_{conv} < \tau_{diff}$, there is not enough time for the solute to diffuse within the water stream, while when $\tau_{conv} \geq \tau_{diff}$, the solute would have sufficient time to diffuse and the radial concentration would be uniform across the channel. For 0.55 ml/min aqueous inlet flow rate $\tau_{conv} \approx \tau_{diff}$, indicating that for aqueous inlet flow rates up to 0.55 ml/min there would be sufficient time for the complete mixing of the reacting species.

Operation of the membrane separator

For the separation of the organic phase (heptane) from the aqueous solution containing the synthesised Au NPs, an in-house designed membrane separator made of PEEK and using

a hydrophobic PTFE membrane was connected downstream of the synthesis reactor. (average pore size: 0.2 μm, Sterlitech Corporation) (Fig. 3). Previous literature studies have implemented and investigated the use of PTFE membrane separators in continuous flow syntheses as they have various advantages over other separators (e.g., gravity separators, microcapillary arrays) [33–35]: (1) PTFE offers broad chemical compatibility and it can be implemented in a wide area of chemical syntheses. (2) They are scalable up to small-scale flow chemistry applications and therefore a suitable candidate for the development of continuous manufacturing platforms. (3) The membrane separators are easy to fabricate and use. (4) Due to the small average pore diameter (0.1–10 μm), they can be used for the separation of liquids with low interfacial tension.

The membrane separator was tested for a range of inlet flow rates and backpressures to map the optimum operating conditions for the successful continuous separation of the heptane and aqueous Au NPs solution. An experimental visual inspection was conducted using blue dye in the aqueous phase and heptane to evaluate the liquid-liquid separation (or the retention and breakthrough), within a range of different inlet flow rates and applied pressures. The total flow rate ($\dot{V}_{Total}$) varied between 0.1 and 1.0 ml/min, where $\dot{V}_{Blue} = \dot{V}_{Organic} = \dot{V}_{Total}/2$. The applied pressure on the system (on the aqueous phase outlet) ranged between 0 and 2 barg using a backpressure regulator (K-type, Swagelok), while the heptane phase outlet was at ambient pressure. The pressure in the aqueous stream was monitored using a digital pressure test gauge (Druck DPI 104, General Electric). There was a 0.2 barg pressure drop at the aqueous phase for the maximum inlet flow rate used ($\dot{V}_{Total}$ = 1.0 ml/min), while the maximum applied pressure did not exceed 2 barg to avoid breakage of glass collection vials at the outlet of the membrane separator (Duran 100 ml, Schott). The experiments indicated successful separation of the two immiscible liquids within the studied flow rates and the applied pressures, indicating that the PTFE membrane could be used as an inline separator for the separation of the heptane and the aqueous Au NPs solution at the outlet of the capillary reactor.

Previous studies have investigated and reported the existence of particle deposition on the capillary and reactor walls during the single-phase synthesis of gold nanoparticles [6, 7, 9]. Huang et al. [7] conducted an in-depth investigation on the fouling of Au NPs on fluorinated capillaries for the Turkevich synthesis and identified two types of fouling, namely the "*dark fouling*" consisting of Au^0, gold ions and citrate-gold complexes due to adsorption on the reactor wall, and the "*pink fouling*" consisting of irreversibly attached formed Au NPs due to van der Waals forces. In this study, after the liquid-liquid separation it is possible that the formed Au NPs might attach on the PTFE membrane causing fouling and loss of material as well as clogging of the membrane after prolonged operation. The synthesis of Au NPs in flow was investigated with and without the use of the membrane separator to identify if fouling takes place, as well as the effect of the membrane separator on the final particle size and shape. Figure 4a shows the offline UV-Vis absorption spectra of the synthesised Au NPs with and without the PTFE membrane separator after operating for one residence time (6.5 min), while Fig. 4b and c show the TEM images of the formed particles with and without the membrane separator, respectively. In both cases – with and without the membrane separator – the absorption spectra were identical. The particle size (based on TEM) was similar and equal to 12.8 ± 1.4 nm and 13.1 ± 1.2 nm without and with the membrane separator, respectively. As previously discussed by Yang et al. [34] and Heider et al. [36], fouling can occur after prolong hours of use of the membrane separator for pharmaceutical products. The Au NPs synthesis process continued for up to 4 h to evaluate if fouling occurs on the membrane over time and the membrane separator was disassembled showing that there was some fouling on the PTFE membrane, after visual inspection (Fig. 5). Fouling was observed at the top part of the membrane separator, which was coming in contact with the aqueous colloidal

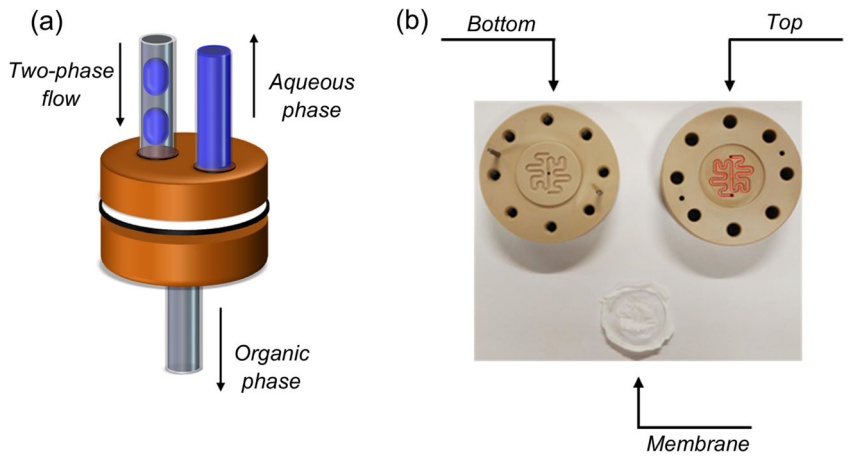

Fig. 3 **a** Schematic representation of the PEEK membrane separator used for the separation of the aqueous and organic phase (heptane) of the two-phase flow system. The aqueous phase is represented by the blue colour. **b** Image of the internal parts of the membrane separator showing the top and bottom parts, the area of separation highlighted in red (channel dimensions on each part: length: 80 mm, width: 1 mm, height: 0.5 mm) and the PTFE membrane used in this study (average pore size, 0.2 μm)

solution. It concentrated at the inlet of the two-phase flow in the membrane separator.

Synthesis of gold nanoparticles in flow

The use of a liquid-liquid biphasic system prevented the particle deposition on the capillary walls due to the organic liquid film forming between the aqueous droplet and the reactor walls, while the segmented flow can approximate plug-flow reactor (PFR) behaviour, since every aqueous droplet acts as an independent batch reactor [37]. The system was tested for the synthesis of 10–20 nm Au NPs. The concentrations of the reactants and the respective flow rates are shown in Table 1. The flow rates were chosen to ensure that reactants would be sufficiently mixed and also considering our previous findings on the required reaction time in batch [24], so that the nominal residence time of the aqueous mixture in the capillary reactor would be enough for the synthesis to be completed.

Figure 6 shows the particle size distribution and UV-Vis spectra obtained from the experiments. The particle size obtained via DCS for experiments A, B and C was 12.2 ± 0.9 nm, 15.2 ± 1.0 nm and 19.3 ± 1.6 nm, respectively, while the particle sizes obtained by TEM were 12.1 ± 2.6 nm, 14.0 ± 1.4 nm and 18.1 ± 1.8 nm, for the targeted synthesis of 10 nm, 15 nm and 20 nm, respectively (Fig. 6c-e). The respective TEM results in batch for the A, B and C experiments were 10.8 ± 1.2 nm, 15.0 ± 1.0 nm and 18.4 ± 1.5 nm, respectively [24]. There seems to be an agreement between the batch and

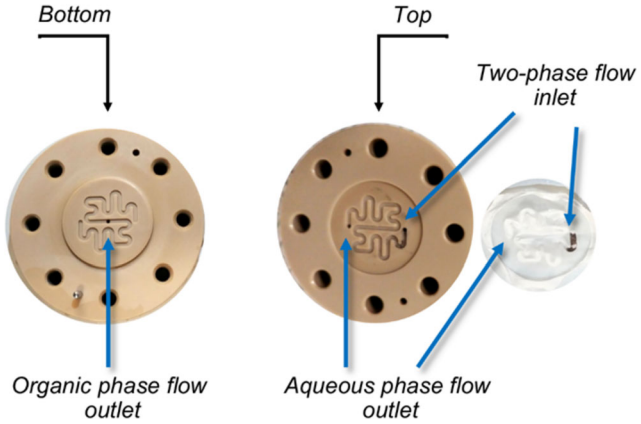

Fig. 5 Top and bottom parts of the membrane separator made of PEEK. Fouling observed on the PTFE membrane and the top part of the separator, after 4 h of continuous synthesis of gold nanoparticles. Reactant concentration after mixing: $[HAuCl_4]$, 0.23 mM; $[H_3Ct]$, 0.21 mM; $[Na_3Ct]$, 1.17 mM; temperature, 95 °C; $\dot{V}_{HAuCl_4} = \dot{V}_{H_3Ct:Na_3Ct}$, 0.09 ml/min; $\dot{V}_{Heptane}$, 0.174 ml/min; reactor volume, 2.25 ml; residence time, 6.5 min; average pore size of the PTFE membrane, 0.2 μm

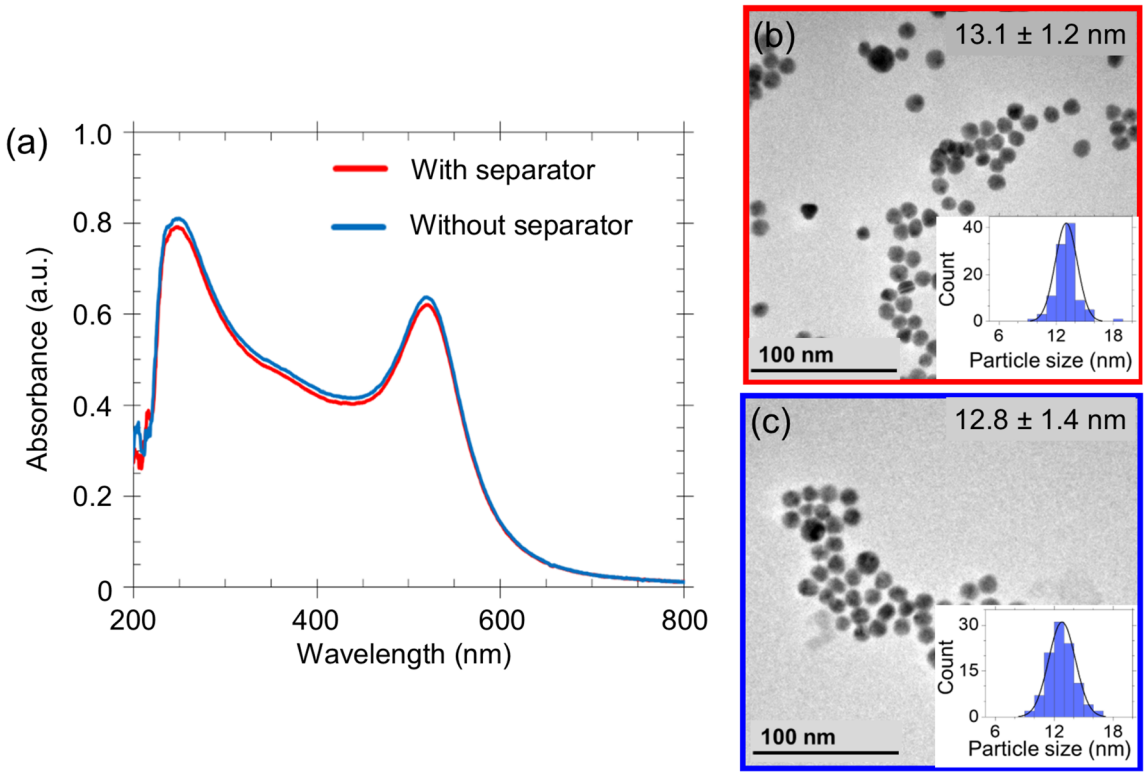

Fig. 4 Offline analysis of the synthesised gold nanoparticles in flow with and without the membrane separator. The operating time with the membrane separation was one residence time (6.5 min). **a** UV-Vis absorption spectra and TEM imaging **b** with and **c** without the membrane separator. Histograms in **b** and **c** show the particle size distribution obtained by TEM. Reactant concentration after mixing: $[HAuCl_4]$, 0.23 mM; $[H_3Ct]$, 0.21 mM; $[Na_3Ct]$, 1.17 mM; temperature, 95 °C; $\dot{V}_{HAuCl_4} = \dot{V}_{H_3Ct:Na_3Ct}$, 0.09 ml/min; $\dot{V}_{Heptane}$, 0.174 ml/min; reactor volume, 2.25 ml; residence time, 6.5 min; average pore size of the PTFE membrane, 0.2 μm

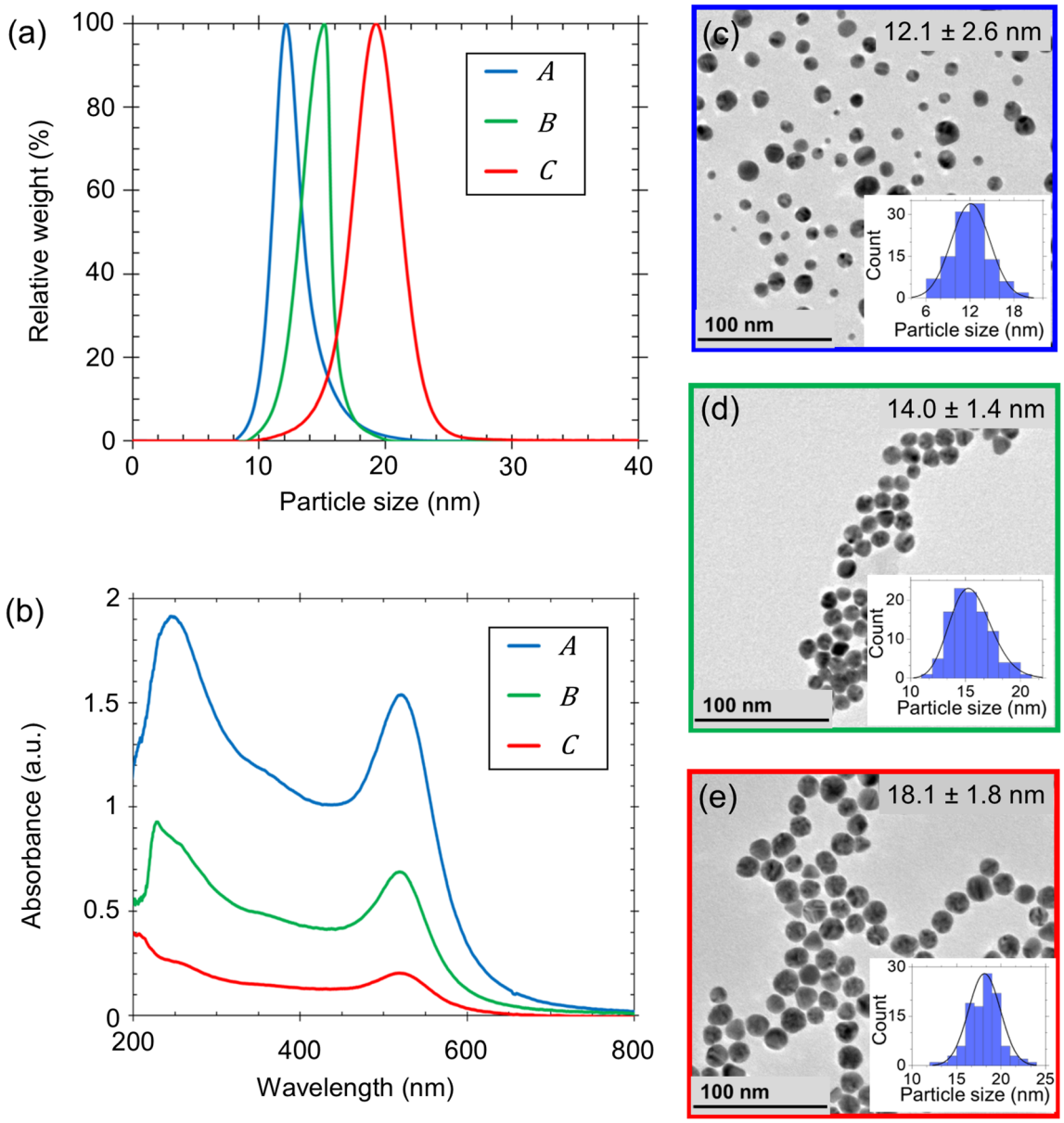

Fig. 6 **a** Particle size distribution (obtained by DCS), **b** UV-Vis spectra, **c**-**e** TEM images of the gold nanoparticles for experimental sets A – C, respectively. Results were obtained after operating for one residence time in each experimental set once steady state was ensured. Histograms in (**c**)-(**e**) display the particle size distribution obtained by TEM. Operating conditions are shown in Table 1

flow results for the experimental sets B and C. However, for the experimental set A, the observed discrepancies between the batch and flow experiments and the large polydispersity in flow (~ 22 %) may be due to the larger reactor entrance length required for temperature stabilisation. There was no fouling observed on the PTFE walls of the coiled capillary mixer due to the fact that the synthesis is very slow at room temperature. Figure S2 (Supplementary Information) shows the coiled capillary mixer, where fouling can be observed only after the reactants were left in the capillary overnight. In order to evaluate any entrance effect for temperature profile stabilisation, Figure S3 (Supplementary Information) shows the temperature profile for single-phase flow of water and heptane through the PTFE capillary (inner diameter: 1 mm) at high flow rate ($\dot{V}_{Heptane} = \dot{V}_{Aqueous}$ = 0.5 ml/min). The targeted temperature of 95 °C was reached ~ 20 cm from the inlet for water and 10 cm for heptane, which translates to 3–6 % of the overall reactor length (~ 287 cm). However, in this work, a two-phase flow system was introduced, where the heat transfer to the aqueous phase is enhanced due to the internal vortices and the recirculation in the moving aqueous droplets [38–40]. Thus, the temperature in the aqueous droplet and the heptane slug was expected to reach 95 °C faster than compared to the single-phase system and the establishing

longitudinal temperature profile at the capillary inlet should have only small (if any) effect on the Au NPs synthesis process.

As discussed above, the experimental conditions for the 10–20 nm Au NPs were based on our previous study for the synthesis of the same size range in batch [24], while targeting the solution pH at ~ 5.6 to ensure high reproducibility of the process [23]. For the flow synthesis, there could have been variations in the pH in the formed aqueous droplets because of flow fluctuations by the pump during the process, as well as due to experimental inaccuracies. The study of Contreras-Trigo et al. [41] has shown that small variation on the pH in the citrate reduction method (from 4.7 to 5.3) can alter the average particle size between ~ 14.0 nm – 15.5 nm, due to the shift on the gold complex and citrate species taking part in the reactions at different pH [23]. The pH of the solution could also be affected by reactant speciation in the initial part of the reactor where the solution temperature increases from room temperature to the target of 95 °C; the species of gold and citrate will be different than those expected at the final temperature (as the redistribution of the reactants among their various species is temperature-dependent) [42, 43]. This can potentially cause a change in the particle formation rate as compared to the equivalent batch experiments, leading to the minor discrepancies observed.

Proof of concept for a continuous manufacturing platform

To establish an online quality control system and develop a continuous manufacturing set-up [4], the syringe pumps were replaced by milliGAT HF piston pumps (Global FIA) and an online UV-Vis spectrometer was positioned at the aqueous stream outlet of the membrane separator. The Au NPs colloidal solution passed through a flow-through cell and the UV-Vis absorbance spectra were recorded in time (Section S5, Supplementary Information). The process stability was evaluated by recording the position (λ_{SPR}) and the absorbance (A_{SPR}) of the surface plasmon resonance (SPR) peak, while the particle size (in nm) was estimated based on the model developed by Haiss et al. [44] for particle sizes above 5 nm:

$$d_{est} = \exp\left(B_1 \frac{A_{SPR}}{A_{450}} - B_2\right) \quad (3)$$

where A_{SPR} is the absorbance of the SPR peak, A_{450} is the absorbace at 450 nm wavelength of the UV-Vis spectra, and B_1 and B_2 are experimentally derived fitting factors equal to 3 and 2.2, respectively.

The position of the SPR peak is characteristic of the particle size and shape, however, increasing sample polydispersity could broaden the peak or cause red-shifting [45]. Additionally, the yield of the Au NPs synthesis process was estimated via the UV-Vis spectra using the Beer-Lambert law as described by Hendel et al. [45] and Yue et al. [13] The concentration of Au^0 in the colloidal solution was calculated via the absorbance at 400 nm (A_{400}) and the yield (Y) was estimated by the ratio of the concentration of the Au^0 in the colloidal solution over the concentration of gold after mixing:

$$A_{400} = \epsilon_{ext,400} \cdot \left[Au^0\right] \cdot l \quad (4)$$

$$Y = \frac{\left[Au^0\right]}{[HAuCl_4]_{target}} \quad (5)$$

where A_{400} is the absorbance of the UV-vis spectra at 400 nm, $\epsilon_{ext,400}$ is the extinction coefficient of Au NPs (ranging between 2.29 and 2.38 L/mol·cm for 10–20 nm citrate-capped Au NPs) [45], $\left[Au^0\right]$ is the concentration of the Au^0 in the colloidal solution, l is the length of the flow-through cuvette used in the UV-Vis measurement (1 cm) and $[HAuCl_4]_{target}$ is the target concentration of the gold precursor after mixing.

Figure 7 show the particle size during 2 h of continuous operation, obtained via TEM imaging and DCS and the calculated values from Eq. 3 via UV-Vis spectroscopy for targeted particle sizes between 10–20 nm Au NPs size. Figures S4 a-c (Supplementary Information) show that the position of the SPR peak in all syntheses was located between 515 nm – 525 nm, indicating the formation of spherical Au NPs of 10–20 nm in size [44]. The particle size and the process yield were measured experimentally via DCS, TEM and MP-AES was used to evaluate the accuracy of the online monitoring using the UV-Vis spectra. For experimental runs A and B Figs. 7 and 8 show that the particles had a monomodal distribution and the obtained sizes over time – via DCS – were 13.9 ± 3.5 nm, 12.6 ± 1.8 nm, 12.4 ± 2.0 nm, 12.4 ± 1.8 nm for run A and 14.7 ± 2.3 nm, 14.9 ± 2.2 nm, 14.9 ± 2.2 nm, 14.6 ± 2.1 nm for run B, at 30 min, 60 min, 90 and 120 min, respectively. Similarly, the particle size obtained by TEM over the 2 h run fluctuated around 12.9 nm (Figs. 7) and 15.2 nm (Fig. 8), respectively, which was similar to the particle size obtained in the first experimental test (Fig. 6). It is worth noting that the particle size of the experimental run A and B over time obtained by TEM and DCS was similar and the aspect ratio of the colloidal solutions was ~ 1.1 indicating spherical particles. Comparing the aforementioned Au NPs for run A and B with the previously synthesised particles in Fig. 6, the synthesis showed high reproducibility, as there was less than 1 nm difference in particle size in each case. The polydispersity ranged between 10–12 %, as obtained by TEM imaging over time, except for the particle size of the experimental run A at 30 min (Fig. 7c), where the polydispersity was

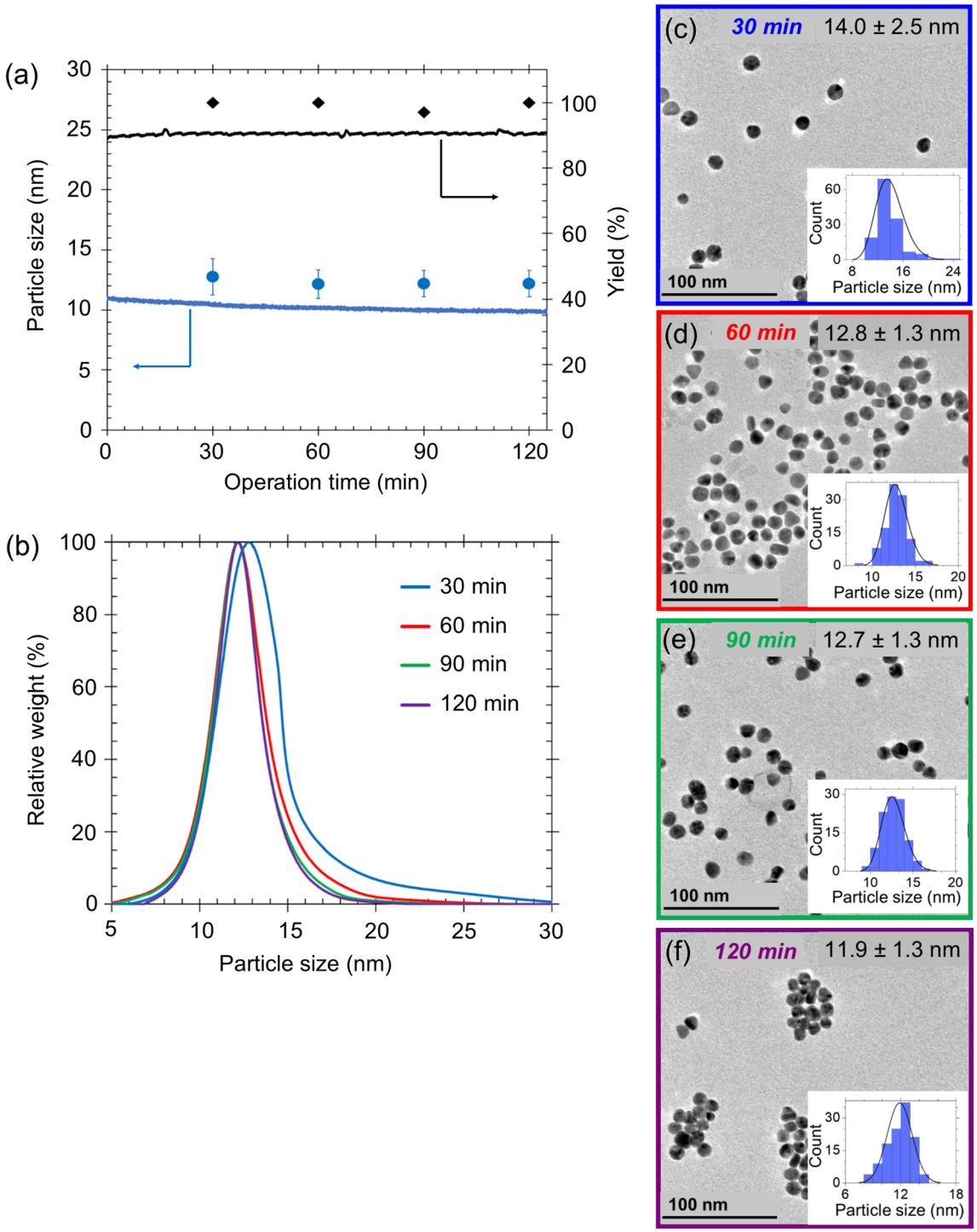

Fig. 7 **a** Particle size and yield of the gold nanoparticle synthesis for experimental run A over 120 min operation time. Solid lines: experimental values obtained via online UV-Vis spectroscopy. Marks: experimental values obtained via TEM imaging (circles) and MP-AES (diamonds). **b** Particle size distribution of the gold nanoparticles over 120 min operation time, obtained by DCS. c-f) TEM images of the gold nanoparticles, obtained via TEM imaging, after **c** 30 min, **d** 60 min, **e** 90 min and **f** 120 min operation time. Histograms in (**c**)-(**f**) display the particle size distribution obtained by TEM. Operating conditions are shown in Table 1

~18 % and comparable to the high polydispersity observed for the initial attempt of the same experimental run (21 %) shown in Fig. 6c. The high polydispersity could be related to the deviation of the pH of the collected colloidal solution from the target pH of ~5.6, as the pH of the colloidal solution was ~5.3 when the particle polydipersity was between 18–21 %. The discrepancy of the pH could be attributed to the reasons discussed

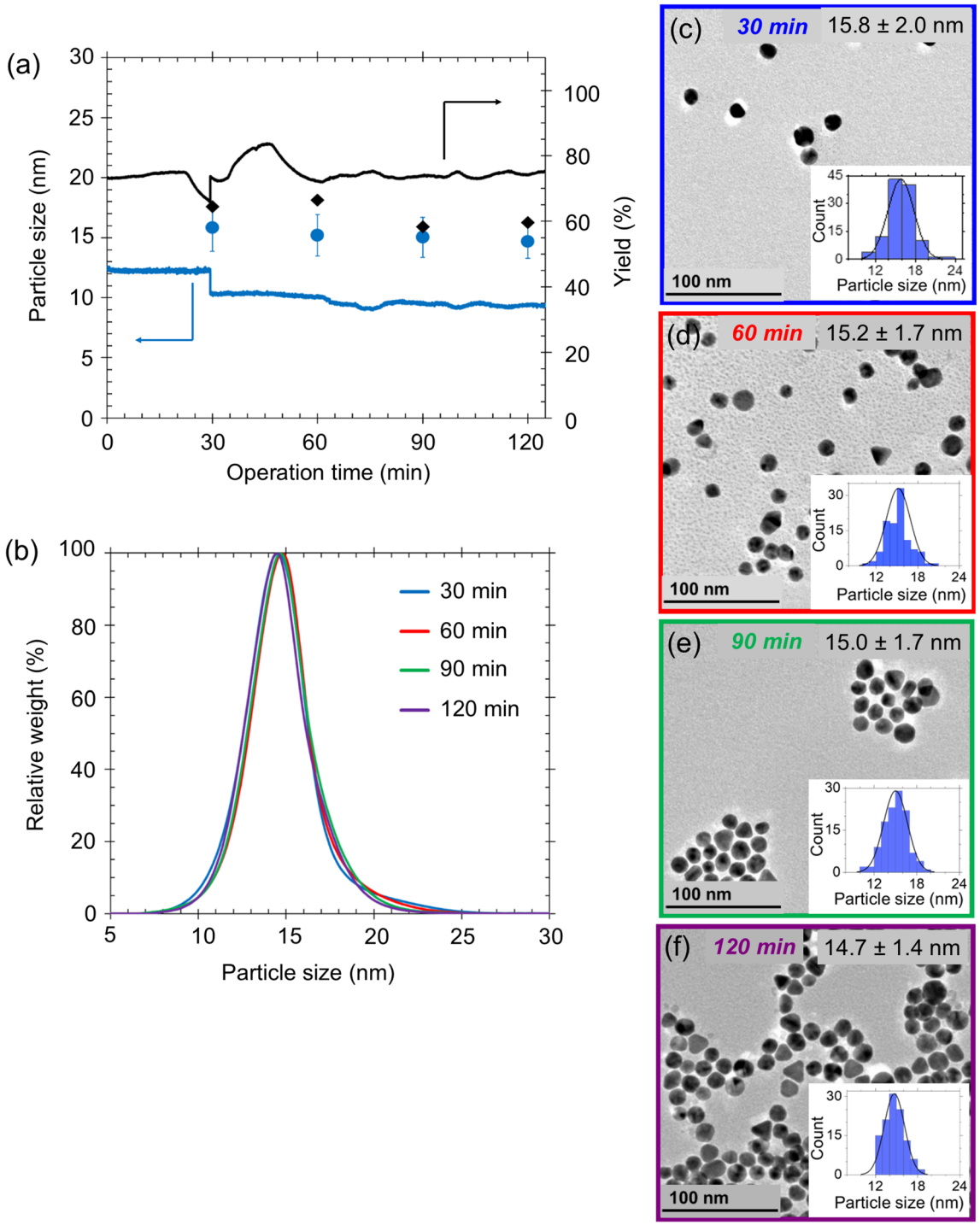

Fig. 8 **a** Particle size and yield of the gold nanoparticle synthesis for experimental run B over 120 min operation time. Solid lines: experimental values obtained via online UV-Vis spectroscopy. Marks: experimental values obtained via TEM imaging (circles) and MP-AES (diamonds). **b** Particle size distribution of the gold nanoparticles over 120 min operation time, obtained by DCS. c-f) TEM images of the gold nanoparticles, obtained via TEM imaging, after **c** 30 min, **d** 60 min, **e** 90 min and **f** 120 min operation time. Histograms in (**c**)-(**f**) display the particle size distribution obtained by TEM. Operating conditions are shown in Table 1.

above i.e., including fluctuations on the flow rates and different speciation equilibrium due to the longitudinal temperature profile in the capillary reactor.

There was a discrepancy between estimated particle size from Eq. 3 and the experimental data obtained by TEM, as the particle size in Fig. 7 ranged between

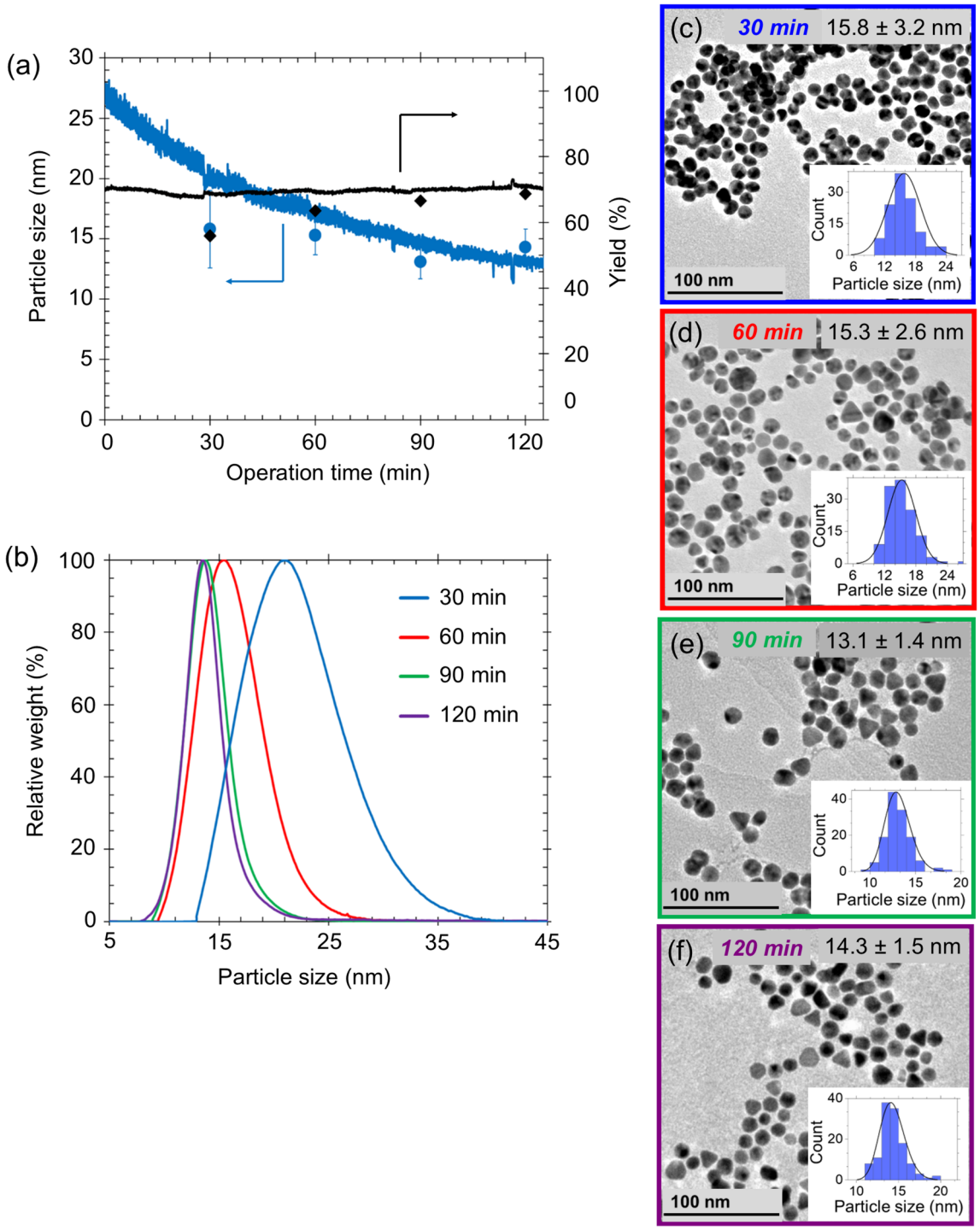

Fig. 9 **a** Particle size and yield of the gold nanoparticle synthesis for experimental run C over 120 min operation time. Solid lines: experimental values obtained via online UV-Vis spectroscopy. Marks: experimental values obtained via TEM imaging (circles) and MP-AES (diamonds). **b** Particle size distribution of the gold nanoparticles over 120 min operation time, obtained by DCS. c-f) TEM images of the gold nanoparticles, obtained via TEM imaging, after **c** 30 min, **d** 60 min, **e** 90 min and **f** 120 min operation time. Histograms in (**c**)-(**f**) display the particle size distribution obtained by TEM. Operating conditions are shown in Table 1

11.0 nm (at the beginning of the operation time) and 9.7 nm (120 min operation time), while the particle size in Fig. 8 ranged between 12.4 nm (at the beginning of the operation time) and 9.4 nm (120 min operation time). The size (d_{est}) obtained by UV-Vis was 16–37 % lower as compared to that from the TEM data. The model by Haiss et al. [44] was developed for perfectly spherical nanoparticles. Therefore the polydispersity of samples as

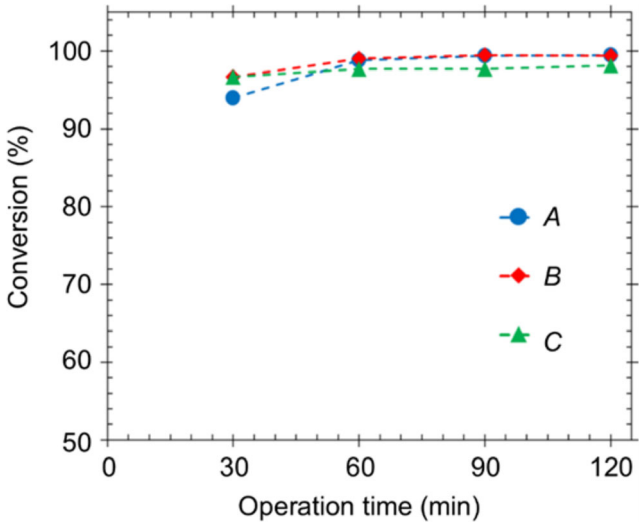

Fig. 10 Conversion of the nanoparticle synthesis experiments (runs A – C) over 2 h operation time, obtained by MP-AES. Operating conditions are shown in Table 1

well as their sphericity of ~ 1.1 (as found by TEM), could affect the evaluation and accuracy of the method due to the shift of the UV-Vis spectra [44, 46, 47].

Interestingly, for the experimental run C (Fig. 9), as shown by the DCS over time, although Au NPs size after 30 min (21.6 ± 4.7 nm) was similar with the synthesised particles (run C) in Fig. 6a, there was a decrease of the particle size during the 2 h run to 16.1 ± 3.2 nm (60 min), 14.2 ± 2.3 nm (90 min) and 14 ± 2.5 nm (120 min). A similar trend can be observed on the estimated particle size by the online UV-Vis spectroscopy (Fig. 9a). The estimated particle size in this case decreased from 27.9 nm to 13.4 nm. The decrease of the particle size during the 2 h operation can be confirmed also by the blue-shifting of the SPR peak location from 526 nm to 524 nm (Figure S4c Supplementary Information). The reason is unclear but could be related to the temperature along the reactor not reaching steady state (due to the low flow rates used) or to insufficient speciation of the precursor in the beginning of the operation, which speciated over time in the stock vial allowing the process to reach steady-state. The pH of the colloidal solution at 30 min operation time was measured to be 4.15, while after 60 min, it was 5.35. Wuithschick et al. [42] recommended the boiling the gold precursor prior to the Au NPs synthesis in batch to ensure sufficient speciation, but this could not be implemented in our flow configuration due to fouling issues in the mixing stage. There seems to be a large discrepancy between the obtained size for 30 min operation time between DCS (21.0 ± 7.7 nm) and TEM (15.8 ± 2.0 nm), the discrepancy could be related to the influence of agglomerated particles on the size distribution provided by DCS, since the instrument calculates the agglomerates as spheres with equivalent diameter and sedimentation time depending on the size, shape and configuration of every agglomerate [48].

In order to evaluate the robustness of the manufacturing platform over the 2 h run, the yield of the Au NPs synthesis with time was evaluated using Eq. 5 via online UV-Vis monitoring and experimentally via MP-AES. In all syntheses described above and shown in Figs. 7, 8 and 9, the conversion obtained by MP-AES was between 94 and 99 %, confirming that the synthesis was completed within the targeted residence times in the capillary reactor, as shown in Fig. 10. It is worth noting that the lower conversion was observed for 30 min operation time for all experimental runs A – C, indicating that the synthesis required ~ 60 min to reach a steady state. As shown in Fig. 7 for experiment A, the experimental yield over the 2 h run ranged between 97 and 100 %. The estimated yield via online UV-Vis was almost constant (< 1 % fluctuation) and varied between 89 and 92 %. Changing the operating conditions for the experiment B and C (Figs. 8 and 9), the estimated yield of the Au NPs via online UV-Vis decreased to ~ 70 %, while the discrepancy between the experimental and the estimated yield was again ~ 10 %. Observing the estimated yield over the 2 h run in Fig. 8 (solid black line), there was a large fluctuation at around 30 min, however, similar trend can be observed by the monitoring of the SPR peak (Figure S4b, Supplementary Information) and it is attributed to disturbances in the UV-Vis measurement during sample collection.

Since there was no fouling in the capillary walls, < 100 % yields could be related with the fouling on the membrane separator. The fouling was more severe for experimental runs B and C, likely due to the lower flow rates resulting to longer residence times in the separator. It is worth noting that the accuracy of the yield estimated via the online UV-Vis monitoring is based on an empirical correlation using monodispersed samples [45]. Therefore, the particle size and the sample polydispersity would affect the UV-Vis spectra and the extinction coefficient of the sample, and hence the estimated results. The extinction coefficient increases with particle size, affecting the absorbance A_{400} [45]. The extinction coefficient is proportional to the particle size (and particle volume, d^3) and the sample concentration, hence the absorbance of the spectra (and subsequently A_{400}) decreases by increasing the polydispersity of the sample [49, 50]. Thus, the observed lower values in the process yield could be related to the fouling in the membrane separator, but may be also affected by the properties of the colloidal solution. Nevertheless, the online model showed sufficient qualitative and quantitative agreement on particle size and yield, establishing that online UV-Vis spectroscopy could be used as a quality control technique for live evaluation of a manufacturing process of Au NPs.

Conclusions

This work describes the translation of targeted 10–20 nm gold nanoparticle synthesis from batch to continuous flow. The

synthesis protocol was based on previous batch experiments, where the required reactant concentrations, temperature and reaction time were identified. A two-phase (water/heptane) flow was employed, and fouling of the reactor was avoided due to the protection of the reactor wall by heptane. A PTFE membrane separator permitted the separation of the aqueous (containing the colloidal Au NPs) and the organic (heptane) streams in flow. The synthesised nanoparticles were monitored by an online UV-Vis spectrometer on the aqueous outlet of the membrane separator. UV-Vis spectra acquisition via online monitoring over a 2 h synthesis run allowed the assessment of the process stability and particle size. The observed discrepancies between the experimentally measured particle sizes and the estimated ones using a literature regression model based on UV-Vis spectra were attributed to the deviation from sphericity and the polydispersity of the produced Au NPs. The process yield was evaluated experimentally offline, as well as online via UV-Vis and exhibited a ~ 10 % discrepancy between the two evaluation methods. The current system provides a new approach on continuous gold nanoparticle synthesis integrated with online monitoring for live quality control.

Supplementary Information The online version contains supplementary material available at https://doi.org/10.1007/s41981-021-00172-3.

Acknowledgements The authors thank the EPSRC (EP/M015157/1) through the Manufacturing Advanced Functional Materials (MAFuMa) scheme and the DST-UKIERI 2017 18 − 017 (contract IND/CONT/G/17–18/47) scheme for financial support.

Declarations

Conflict of interest There are no conflicts to declare.

References

1. Shen J-J, Zhang P-H, Zheng F, Chen H, Chen W, Ding Y, Xia X-H (2018) Preliminary quality criteria of citrate-protected gold nanoparticles for medicinal applications. ACS Appl Nano Mater 1(5):2120–2128
2. Sengani M, Grumezescu AM, Rajeswari VD (2017) Recent trends and methodologies in gold nanoparticle synthesis – A prospective review on drug delivery aspect. OpenNano 2:37–46
3. Macdonald TJ, Wu K, Sehmi SK, Noimark S, Peveler WJ, du Toit H, Voelcker NH, Allan E, MacRobert AJ, Gavriilidis A, Parkin IP (2016) Thiol-capped gold nanoparticles swell-encapsulated into polyurethane as powerful antibacterial surfaces under dark and light conditions. Sci Rep 6:39272
4. Stavis SM, Fagan JA, Stopa M, Liddle JA (2018) Nanoparticle manufacturing – Heterogeneity through processes to products. ACS Appl Nano Mater 1(9):4358–4385
5. deMello J, deMello A (2004) Microscale reactors: nanoscale products. Lab Chip 4(2):11N-15N
6. Wagner J, Köhler JM (2005) Continuous synthesis of gold nanoparticles in a microreactor. Nano Lett 5(4):685–691
7. Huang H, du Toit H, Besenhard MO, Ben-Jaber S, Dobson P, Parkin I, Gavriilidis A (2018) Continuous flow synthesis of ultrasmall gold nanoparticles in a microreactor using trisodium citrate and their SERS performance. Chem Eng Sci 189:422–430
8. Krishna KS, Li Y, Li S, Kumar CSSR (2013)Lab-on-a-chip synthesis of inorganic nanomaterials and quantum dots for biomedical applications. Adv Drug Deliv Rev 65(11):1470–1495
9. Lohse SE, Eller JR, Sivapalan ST, Plews MR, Murphy CJ (2013) A simple millifluidic benchtop reactor system for the high-throughput synthesis and functionalization of gold nanoparticles with different sizes and shapes. ACS Nano 7(5):4135–4150
10. Długosz O, Banach M (2019) Continuous production of silver nanoparticles and process control. J Cluster Sci 30(3):541–552
11. Naidu S, Sawhney R, Li X (2008) A methodology for evaluation and selection of nanoparticle manufacturing processes based on sustainability metrics. Environ Sci Technol 42(17):6697–6702
12. Cattaneo S, Althahban S, Freakley SJ, Sankar M, Davies T, He Q, Dimitratos N, Kiely CJ, Hutchings GJ (2019) Synthesis of highly uniform and composition-controlledgold–palladium supported nanoparticles in continuous flow. Nanoscale 11(17):8247–8259
13. Yue J, Falke FH, Schouten JC, Nijhuis TA (2013) Microreactors with integrated UV/Vis spectroscopic detection for online process analysis under segmented flow. Lab Chip 13(24):4855–4863
14. Baber R, Mazzei L, Thanh NTK, Gavriilidis A (2017) An engineering approach to synthesis of gold and silver nanoparticles by controlling hydrodynamics and mixing based on a coaxial flow reactor. Nanoscale 9(37):14149–14161
15. Panariello L, Mazzei L, Gavriilidis A (2018) Modelling the synthesis of nanoparticles in continuous microreactors: The role of diffusion and residence time distribution on nanoparticle characteristics. Chem Eng J 350:1144–1154
16. Ahmed B, Barrow D, Wirth T (2006) Enhancement of reaction rates by segmented fluid flow in capillary scale reactors. Adv Synth Catal 348(9):1043–1048
17. Duraiswamy S, Khan SA (2009)Droplet-based microfluidic synthesis of anisotropic metal nanocrystals. Small 5(24):2828–2834
18. Sebastian Cabeza V, Kuhn S, Kulkarni AA, Jensen KF (2012)Size-controlled flow synthesis of gold nanoparticles using a segmented flow microfluidic platform. Langmuir 28(17):7007–7013
19. Kulkarni AA, Sebastian Cabeza V (2017) Insights in the diffusion controlled interfacial flow synthesis of Au nanostructures in a microfluidic system. Langmuir 33(50):14315–14324
20. Carino A, Walter A, Testino A, Hofmann H (2016) Continuous synthesis of gold nanoparticles using the segmented flow tubular reactor (SFTR). CHIMIA Int J Chem 70(6):457–457
21. Mondini S, Ferretti AM, Puglisi A, Ponti A (2012) Pebbles and PebbleJuggler: Software for accurate, unbiased, and fast measurement and analysis of nanoparticle morphology from transmission electron microscopy (TEM) micrographs. Nanoscale 4(17):5356–5372
22. du Toit H, Macdonald TJ, Huang H, Parkin IP, Gavriilidis A (2017) Continuous flow synthesis of citrate capped gold nanoparticles using UV induced nucleation. RSC Adv 7(16):9632–9638
23. Kettemann F, Birnbaum A, Witte S, Wuithschick M, Pinna N, Kraehnert R, Rademann K, Polte J (2016) Missing piece of the

mechanism of the Turkevich method: The critical role of citrate protonation. Chem Mater 28(11):4072–4081
24. Damilos S (2020) Development of flow reactors for tuneable gold nanoparticle synthesis: Towards continuous manufacturing (Doctoral thesis). University College London, London, UK
25. Shui L, Eijkel JC, van den Berg A (2007) Multiphase flow in microfluidic systems - Control and applications of droplets and interfaces. Adv Colloid Interface Sci 133(1):35–49
26. Garstecki P, Fuerstman MJ, Stone HA, Whitesides GM (2006) Formation of droplets and bubbles in a microfluidic T-junction—Scaling and mechanism of break-up. Lab Chip 6(3):437–446
27. Bruus H (2008) Microfluidics T. Oxford University Press, Oxford
28. Aussillous P, Quéré D (2000) Quick deposition of a fluid on the wall of a tube. Phys Fluids 12(10):2367–2371
29. Nguyen N-T, Wu Z (2004)Micromixers—A review. J Micromech Microeng 15(2):R1–R16
30. Rossi D, Gargiulo L, Valitov G, Gavriilidis A, Mazzei L (2017) Experimental characterization of axial dispersion in coiled flow inverters. Chem Eng Res Des 120:159–170
31. Klutz S, Kurt SK, Lobedann M, Kockmann N (2015) Narrow residence time distribution in tubular reactor concept for Reynolds number range of 10–100. Chem Eng Res Des 95:22–33
32. Hariri MB, Dolati A, Moakhar RS (2013) The potentiostatic electrodeposition of gold nanowire/nanotube in HAuCl4 solutions based on the model of recessed cylindrical ultramicroelectrode array. J Electrochem Soc 160(6):D279–D288
33. Adamo A, Heider PL, Weeranoppanant N, Jensen KF (2013) Membrane-based, liquid–liquid separator with integrated pressure control. Ind Eng Chem Res 52(31):10802–10808
34. Yang L, Weeranoppanant N, Jensen KF (2017) Characterization and modeling of the operating curves of membrane microseparators. Ind Eng Chem Res 56(42):12184–12191
35. Kralj JG, Sahoo HR, Jensen KF (2007) Integrated continuous microfluidic liquid–liquid extraction. Lab Chip 7(2):256–263
36. Heider PL, Born SC, Basak S, Benyahia B, Lakerveld R, Zhang H, Hogan R, Buchbinder L, Wolfe A, Mascia S, Evans JMB, Jamison TF, Jensen KF (2014) Development of a multi-step synthesis and workup sequence for an integrated, continuous manufacturing process of a pharmaceutical. Org Process Res Dev 18(3):402–409
37. Jongen N, Donnet M, Bowen P, Lemaître J, Hofmann H, Schenk R, Hofmann C, Aoun-Habbache M, Guillemet-Fritsch S, Sarrias J, Rousset A, Viviani M, Buscaglia MT, Buscaglia V, Nanni P, Testino A, Herguijuela JR (2003) Development of a continuous segmented flow tubular reactor and the "scale-out" concept – In search of perfect powders. Chem Eng Technol 26(3):303–305
38. Gupta R, Fletcher DF, Haynes BS (2010) CFD modelling of flow and heat transfer in the Taylor flow regime. Chem Eng Sci 65(6): 2094–2107
39. Dai Z, Guo Z, Fletcher DF, Haynes BS (2015) Taylor flow heat transfer in microchannels—Unification of liquid–liquid and gas–liquid results. Chem Eng Sci 138:140–152
40. Gupta R, Leung SSY, Manica R, Fletcher DF, Haynes BS (2013) Hydrodynamics of liquid–liquid Taylor flow in microchannels. Chem Eng Sci 92:180–189
41. Contreras-Trigo B, Díaz-García V, Guzmán-Gutierrez E, Sanhueza I, Coelho P, Godoy SE, Torres S, Oyarzún P (2018) Slight pH fluctuations in the gold nanoparticle synthesis process influence the performance of the citrate reduction method. Sensors 18(7): 2246
42. Wuithschick M, Birnbaum A, Witte S, Sztucki M, Vainio U, Pinna N, Rademann K, Emmerling F, Kraehnert R, Polte J (2015) Turkevich in new robes: Key questions answered for the most common gold nanoparticle synthesis. ACS Nano 9(7):7052–7071
43. Peck JA, Tait CD, Swanson BI, Brown GE (1991) Speciation of aqueous gold(III) chlorides from ultraviolet/visible absorption and Raman/resonance Raman spectroscopies. Geochim Cosmochim Acta 55(3):671–676
44. Haiss W, Thanh N, Aveyard J, Fernig D (2007) Determination of size and concentration of gold nanoparticles from UV-vis spectra. Anal Chem 79(11):4215
45. Hendel T, Wuithschick M, Kettemann F, Birnbaum A, Rademann K, Polte J (2014) In situ determination of colloidal gold concentrations with UV–vis spectroscopy: limitations and perspectives. Anal Chem 86(22):11115–11124
46. Khlebtsov NG (2008) Determination of size and concentration of gold nanoparticles from extinction spectra. Anal Chem 80(17): 6620–6625
47. Amendola V, Meneghetti M (2009) Size evaluation of gold nanoparticles by UV – vis spectroscopy. J Phys Chem C 113(11):4277–4285
48. Minelli C, Sikora A, Garcia-Diez R, Sparnacci K, Gollwitzer C, Krumrey M, Shard AG (2018) Measuring the size and density of nanoparticles by centrifugal sedimentation and flotation. Anal Methods 10(15):1725–1732
49. Amendola V, Pilot R, Frasconi M, Maragò OM, Iatì MA (2017) Surface plasmon resonance in gold nanoparticles: A review. J Phys: Condens Matter 29(20):203002
50. Mulvaney P (1996) Surface plasmon spectroscopy of nanosized metal particles. Langmuir 12(3):788–800